Eur. J. Mineral.
2019, **31**, 575–584
Published online 29 January 2019

Qatranaite, $CaZn_2(OH)_6{\cdot}2H_2O$: a new mineral from altered pyrometamorphic rocks of the Hatrurim Complex, Daba-Siwaqa, Jordan

Yevgeny VAPNIK[1], Evgeny V. GALUSKIN[2,*], Irina O. GALUSKINA[2], Joachim KUSZ[3], Marta STASIAK[2], Tomasz KRZYKAWSKI[1] and Mateusz DULSKI[45]

[1]Department of Geological and Environmental Sciences, Ben-Gurion University of the Negev,
POB 653,
Bear-Sheva 84105, Israel
*Corresponding author, e-mail: evgeny.galuskin@us.edu.pl
[2]Department of Geochemistry, Mineralogy and Petrography, Faculty of Earth Sciences, University of Silesia,
Będzińska 60, 41-200 Sosnowiec, Poland
[3]Institute of Physics, University of Silesia, Uniwersytecka 4, 40-007 Katowice, Poland
[4]Institute of Material Science, 75 Pułku Piechoty 1a, 41-500 Chorzów, Poland
[5]Silesian Center for Education and Interdisciplinary Research, 75 Pułku Piechoty 1a, 41-500 Chorzów, Poland

Abstract: The new mineral qatranaite, $CaZn_2(OH)_6{\cdot}2H_2O$ ($P2_1/c$, $Z = 2$, $a = 6.3889(8)$ Å, $b = 10.9692(14)$ Å, $c = 5.7588(8)$ Å; $\beta = 101.949(14)°$, $V = 394.84(9)$ Å^3; IMA2016-024), was found in cuspidine veins cutting spurrite marble in part of the pyrometamorphic Hatrurim Complex located in the Siwaqa region, Jordan. Qatranaite is the natural counterpart of synthetic calcium hexahydroxodizincate dihydrate. It forms colourless or white crystals up to 0.3 mm in size. Qatranaite is associated with cuspidine, sphalerite, Se-bearing thaumasite, afwillite, calcite, srebrodolskite–brownmillerite, spinel–magnesioferrite, spurrite and fluorapatite–fluorellestadite. The new mineral has an irregular fracture; no cleavage or parting were observed. The calculated density of qatranaite is 2.598 g cm^{-3}, the microhardness $VHN_{25} = 171$ kg mm^{-2} corresponds to ~3.5 in the Mohs' hardness scale. The qatranaite structure is formed by hydroxylated pyroxene-like chains $[Zn_2(OH)_6]^{2-}$, between which the $[Ca(OH_2)_2]^{2+}$ groups are located. The Ca atoms are eight-fold coordinated in $[Ca(OH)_4(OH_2)_2]$ polyhedra which share the four hydroxyl oxygen atoms with the Zn-centred tetrahedra. The main bands in the Raman spectrum of qatranaite are related to vibrations in $Zn(OH)_4^{2-}$ tetrahedra (cm^{-1}): 297, 344 ($\nu_2 + \nu_4$); 440, 449, 479 ($\nu_1 + \nu_3$); 990 (νZn–O–Zn); 1065 (νZn–OH). Strong bands at 3190, 3497 and 3624 cm^{-1} are assigned to OH stretching vibrations. The strongest diffraction lines are [d_{hkl}, Å (I)]: 6.25 (33), 5.002 (14), 3.992 (23), 3.124 (47), 2.881 (100), 2.723 (28), 2.451 (12), 1.575 (20). Qatranaite crystallization was preceded by a high-temperature alteration of spurrite rocks, reflected in the formation of cuspidine along fractures. The formation of qatranaite-bearing veins resulted from low-temperature (<70 °C) rock alteration by hyper-alkaline solutions.

Key-words: Qatranaite; $CaZn_2(OH)_6{\cdot}2H_2O$; new mineral; calcium zincate; hyper-alkaline solutions; electron microprobe; Raman spectroscopy; crystal structure; Daba-Siwaqa; Hatrurim Complex; Jordan.

1. Introduction

Qatranaite, $CaZn_2(OH)_6{\cdot}2H_2O$ (IMA2016-024), was discovered in altered pyrometamorphic spurrite marbles of the Hatrurim Complex in the Daba-Siwaqa region, Jordan (the "Mottled zone"; Bentor, 1960; Gross, 1977; Techer *et al.* 2006; Vapnik *et al.*, 2007; Sokol *et al.*, 2010). The Daba-Siwaqa region is the largest area of the Hatrurim Complex (Geller *et al.*, 2012; Novikov *et al.*, 2013; Khoury *et al.*, 2014). Rocks of the Hatrurim Complex are distributed along the Dead Sea Transform in Israel, Jordan and Palestinian Autonomy. They are represented by exotic clinker-like rocks such as spurrite marbles, larnite pseudo-conglomerates, gehlenite hornfelses and other rarer rocks (Gross, 1977; Novikov *et al.*, 2013; Galuskina *et al.*, 2014; Galuskin *et al.*, 2016). The genesis of the Hatrurim Complex remains under discussion (Sokol *et al.*, 2010; Kolodny *et al.*, 2013; Vapnik & Novikov, 2013; Galuskina *et al.*, 2014). There are two main hypotheses: 1) formation due to combustion of dispersed organic matter (bitumen) within the host sedimentary rocks (Kolodny & Gross, 1974; Matthews & Gross, 1980; Geller *et al.*, 2012) and 2) a mud-volcanic formation hypothesis. The latter suggests pyrometamorphism of the sedimentary protoliths by methane combustion exhaling from tectonically active zones of the Dead Sea Transform (Sokol *et al.*, 2010; Novikov *et al.*, 2013). Recent studies have shown that by-products of the combustion processes, such as gases, fluids and melts generated during pyrometamorphism, reacted with existing minerals. These secondary, but high-temperature

https://doi.org/10.1127/ejm/2019/0031-2833 0935-1221/19/0031-2833 $ 4.50

alterations, allowed for the formation of a significantly greater number of pyrometamorphic minerals than in the common clinker-like association (Galuskina *et al.*, 2014; Galuskin *et al.*, 2015, 2016).

Qatranaite ($P2_1/c$, Z = 2, a = 6.3889(8) Å, b = 10.9692 (14) Å, c = 5.7588(8) Å; β = 101.949(14)°, V = 394.84 (9) Å^3) has a synthetic equivalent named calcium hexahydroxodizincate dihydrate ($CaZn_2(OH)_6{\cdot}2H_2O$, $P2_1/c$, Z = 2, a = 6.372(1) Å, b = 10.940(2) Å, c = 5.749(2) Å, β = 101.94(2)°, V = 392.0 Å^3; Stahl & Jacobs, 1997). Calcium hexahydroxodizincate dihydrate is used as an active material for secondary Zn electrodes utilized in batteries, as precursor catalyst in biodiesel synthesis and as antifungal compound for the protection of limestone monuments (Xavier *et al.*, 2009; Yang *et al.*, 2009; Ropp, 2013; Caldeira *et al.*, 2017).

Qatranaite was named after the village Al Qatrana, which is on the Amman-Aqaba highway 15 km south-east from the type locality. The holotype specimen is deposited in the mineralogical collections of the Fersman Mineralogical Museum in Moscow, Russia, with catalogue number 4855/1.

2. Methods of investigation

The crystal morphology and chemical composition of qatranaite and its associated minerals were examined using optical microscopes, analytical scanning electron microscopes Philips XL30 ESEM/EDAX and Phenom XL (Faculty of Earth Sciences, University of Silesia), and a CAMECA SX100 electron microprobe (Institute of Geochemistry, Mineralogy and Petrology, University of Warsaw). Chemical analyses were carried out on the electron microprobe operated in wavelength dispersive spectrometry mode at 10 kV and 10 nA with a beam size of ~3 μm. The following lines and standards were used: Ca$K\alpha$ – diopside, Zn$L\alpha$ – sphalerite/willemite; contents of F, Al, Si, S, P, Cl, Fe, Mn *etc*. were below detection limit.

The Raman spectra were recorded on a WITec Alpha300 confocal Raman microscope (Institute of Physics, University of Silesia). The excitation laser radiation was coupled to a microscope through a single-mode optical fibre with a diameter of 50 μm. An air Olympus MPLAN (100 ×/ 0.90NA) objective was used. Raman scattered light was focused onto a multimode fibre (50 μm diameter) and monochromator with a 600 line/mm grating. The power of the laser at the sample position was 44 mW. The spectra were accumulated using 15–20 scans with an integration time of 10–15 s and a resolution of 3 cm^{-1}. The spectrometer monochromator was calibrated using the Raman scattering line of a silicon plate (520.7 cm^{-1}).

Single-crystal X-ray studies of qatranaite were carried out using a SuperNova Dual diffractometer with a mirror monochromator (Mo$K\alpha$, λ = 0.71073 Å) and an Atlas CCD detector (Agilent Technologies), at the Institute of Physics, University of Silesia, Poland. The structure of synthetic calcium hexahydroxodizincate dihydrate (Stahl & Jacobs, 1997) was taken as an initial model. The qatranaite structure was refined on the basis of X-ray single-crystal data of 293(2) K to $R1$ = 0.037 using the programme SHELX97 (Sheldrick, 2008).

Fig. 1. Cuspidine veins and "cuspidinised" fragments of spurrite rock (light-grey, white on weathering surface) with qatranaite in non-altered spurrite marble (brown).

Non-hydrogen atoms were refined with anisotropic thermal parameters. Hydrogen atoms were introduced to the structure by appropriate rigid-body constraints with temperature factors U_{iso}(H) equal to 1.5U_{eq}(O); OH distances were restrained to 0.90(5) Å.

The powder X-ray diffraction data were obtained using Panalytical, X'Pert PRO PW3040/60 diffractometer (theta-theta geometry), equipped with a X'Celerator detector with active length (2θ°) of 2.122 at the Faculty of Earth Sciences, University of Silesia, Poland. Experimental parameters were: Cu$K\alpha$ radiation (λ = 1.541874 Å), 50 kV, 40 mA. Data were analysed using the HighScore + programme, v. 4.1. For interpretation, the ICDD PDF 4+ database, v. 2014 was used. The X-ray powder diffraction data for qatranaite are presented in Table S1, freely available in the Supplementary Material linked to this article on the GSW website of the journal: https://pubs.geoscienceworld.org/eurjmin.

3. Occurrence of qatranaite

The type locality of qatranaite (N31°24,23′; E36°15,06′) is situated in the northern part of the Siwaqa pyrometamorphic area, Um Al-Rasas Sub-district, 70 km south-east from Amman, the capital of Jordan. Qatranaite-bearing pyrometamorphic rocks occur as a single outcrop of spurrite marbles, located in the poorly detectable boundary of two lithological units, the Umm Rijam and Muwaqqar Chalk-Marl Formations combined in the Belga Group (Barijous, 1985; Ziegler, 2001; Powell & Moh'd, 2011; Khoury *et al.*, 2014; Abzalov *et al.*, 2015; Alqudah *et al.*, 2015; Sokol *et al.*, 2017). The Eocene Umm Rijam Formation consists of chalky limestone, chalk, chert and microcrystalline limestone with a common thickness of 122 m–145 m (Alsharhan & Nairn, 2003; Fleurance *et al.*, 2013). The Umm Rijam Formation is a stratigraphic equivalent of the Adulam Formation in Israel (Novikov *et al.*, 2013). The Muwaqqar Chalk-Marl

Unit is composed of marl, chalky limestone, micritic limestone and chert. It has been dated to the Maastrichtian to middle Palaeocene. In the lower part of the formation, the bituminous marl is observed, with differentiation of varicoloured marble on top, thickness varies from 70 to 100 m in western outcrops (Khoury *et al.*, 2014; Sokol *et al.*, 2017). The Muwaqqar Chalk-Marl Unit is also a stratigraphic equivalent of Ghareb and Taqiye formations in Israel (Novikov *et al.*, 2013). Sedimentation and diagenesis of the mentioned lithological units took place in a marine environment, during late Cenomanian transgressions until the late Eocene. Due to uplift, as well as tectonic and erosional activity, the precise correlation between the specific rock formations and pyrometamorphic rocks remains unclear. Nevertheless, the presence of disseminated organic matter and elevated concentrations of Cd, Zn, Mo, Ni, V, Cr and U reported from the Muwaqqar Chalk-Marl Formation (Fleurance *et al.*, 2013; Khoury *et al.*, 2014; Abzalov *et al.*, 2015; Sokol *et al.*, 2017) provided the possible source of combustible matter for pyrometamorphism, and acted as the primary Zn source (storage), which evolved later into the formation of diverse Zn-bearing mineralization, including Zn-sulfides and qatranaite.

The area of the Siwaqa is known for mineralogical discoveries, *e.g.*, the new mineral tululite, $Ca_{14}(Fe^{3+},Al)(Al,Zn,Fe^{3+},Si,P,Mn,Mg)_{15}O_{36}$ and the intermediate members of the lime–monteponite solid solutions from spurrite marble (Khoury *et al.*, 2016a and b), as well as terrestrial phosphides from melted rocks (Britvin *et al.*, 2015, 2018a and b).

The diagnostic feature of spurrite rocks from the type locality of qatranaite is an extensive development of the cuspidine veins cutting them, which are up to 10 cm thick (Fig. 1).

In unaltered dark spurrite marbles, calcite content reaches 80 vol%. Apart from spurrite, minerals of the fluorapatite–fluorellestadite and srebrodolskite–brownmillerite series are in significant quantity. Minor and accessory phases are represented by minerals of the fluormayenite–fluorkyuygenite and spinel–magnesioferrite series. Gehlenite, periclase, lakargiite, vorlanite are locally noted in spurrite marble. Also, grains of larnite, zinkite and monteponite are observed. Some parts of spurrite marbles contain elevated concentrations of Zn, Fe, Cu and Ni sulfides, among which sphalerite predominates. Spurrite marbles are crosscut by networks of calcite–thaumasite (rarer ettringite) veins up to 1–2 mm in thickness, around which a bleaching of rock is observed. In the bleaching zones, spurrite is replaced by secondary hydrosilicates (tobermorite-like) and thaumasite; sphalerite is replaced by clinohedrite, $CaZn(SiO_4){\cdot}H_2O$, which also forms narrow veins (Fig. S1, Supplementary Material).

Spurrite marbles in immediate contact with cuspidine veins transform to spurrite rocks as their calcite content falls to a few percents and the rocks bear evidence of recrystallization. This process is reflected in the appearance of spurrite poikilitic crystals (metacrysts) up to 0.5 cm in size in fine-grained (0.01–0.02 mm) spurrite rock (Fig. 2A) or general coarsening of spurrite grains up to 0.2–0.3 mm (Fig. 2B). Recrystallized zones of spurrite rock contain significant amount of sphalerite, which is commonly intergrown with intensively altered Ca–Fe-sulfides and Cu–Fe–Ni-selenides (Fig. 2B). Rarely, unaltered clausthalite, PbSe, and uraniferous garnet of the kerimasite–elbrusite series, $Ca_3(Zr,U,Ti)_2(Fe,Al,Si)_3O_{12}$ (Galuskina *et al.*, 2010; Zaitsev *et al.*, 2011), are observed in these zones.

Table 1. Chemical composition (in wt%) of qatranaite.

Constituent	Mean (n = 10)	S.D.	Range
CaO	17.69	0.31	17.53–17.93
ZnO	52.66	1.34	53.35–54.86
H_2O[a]	28.91		
Sum	99.26		
Ca	0.98		
Zn	2.02		
H	10.00		

[a]Water added stoichiometrically; formula normalized to 3 cations and 8 O *apfu*.

Qatranaite associated with Se-bearing thaumasite, calcite, awfillite and barite was found in secondary low-temperature veins from 10–20 μm to 1–2 mm in thickness (Figs. 2C, D and 3A). Veins with qatranaite occur exclusively in cuspidine zones, where large spurrite crystal relics were observed (Fig. 2C). The cuspidine rock is presented by fine-grained aggregate with grains first tens μm in size, poikilitic crystals of magnesioferrite are observed there (Fig. 2D). As well as recrystallized spurrite rocks, cuspidine zones show higher concentration of sphalerite in comparison with unaltered spurrite marbles (Fig. 2B, D).

4. Physical properties of qatranaite

Qatranaite forms crystals up to 0.3 mm in size. Rare larger crystals are generally poikilitic, with abundant calcite, Se-bearing thaumasite and barite inclusions (Fig. 3B). Qatranaite crystals exhibit the forms: {010}, {110}, {100}, {102}, {112}, {001}, {011}, {10$\bar{1}$}, {10$\bar{2}$} (Figs. 3C, D and 4). Crystals are flattened on (010) and show striations along [001] (Fig. 3D, E). Aggregates of parallel intergrowths of qatranaite crystals a few square millimetres, were detected (Fig. 3E). Sphalerite grains partially replaced by qatranaite were noted in fine-grained cuspidine (Fig. 3F). Qatranaite appears as colourless and white crystals, with a white streak and having a vitreous lustre. Cleavage and parting were not observed. The tenacity is brittle and the fracture is irregular. The abundance of small inclusions of thaumasite, calcite and baryte did not allow for selection of pure grains for accurate density measurement. Density was calculated as 2.598 g cm^{-3} based on its average composition (Table 1). Microhardness, VHN_{25} is in the range 163–178 kg mm^{-2}, with a mean of 171 kg mm^{-2} (from an average of 20 measurements), and corresponds to ~3.5 in the Mohs' scale. Qatranaite is biaxial, negative, non-pleochroic, and has the measured refractive indices (589 nm): α = 1.545(2), β = 1.552(2), γ = 1.554(2). $2V_x$ (meas.) = 45(5)°, $2V_x$ (calc.) = 50.1(1)°, $Z = b$, $X \wedge c \approx 13(2)°$, dispersion: $r > v$, weak.

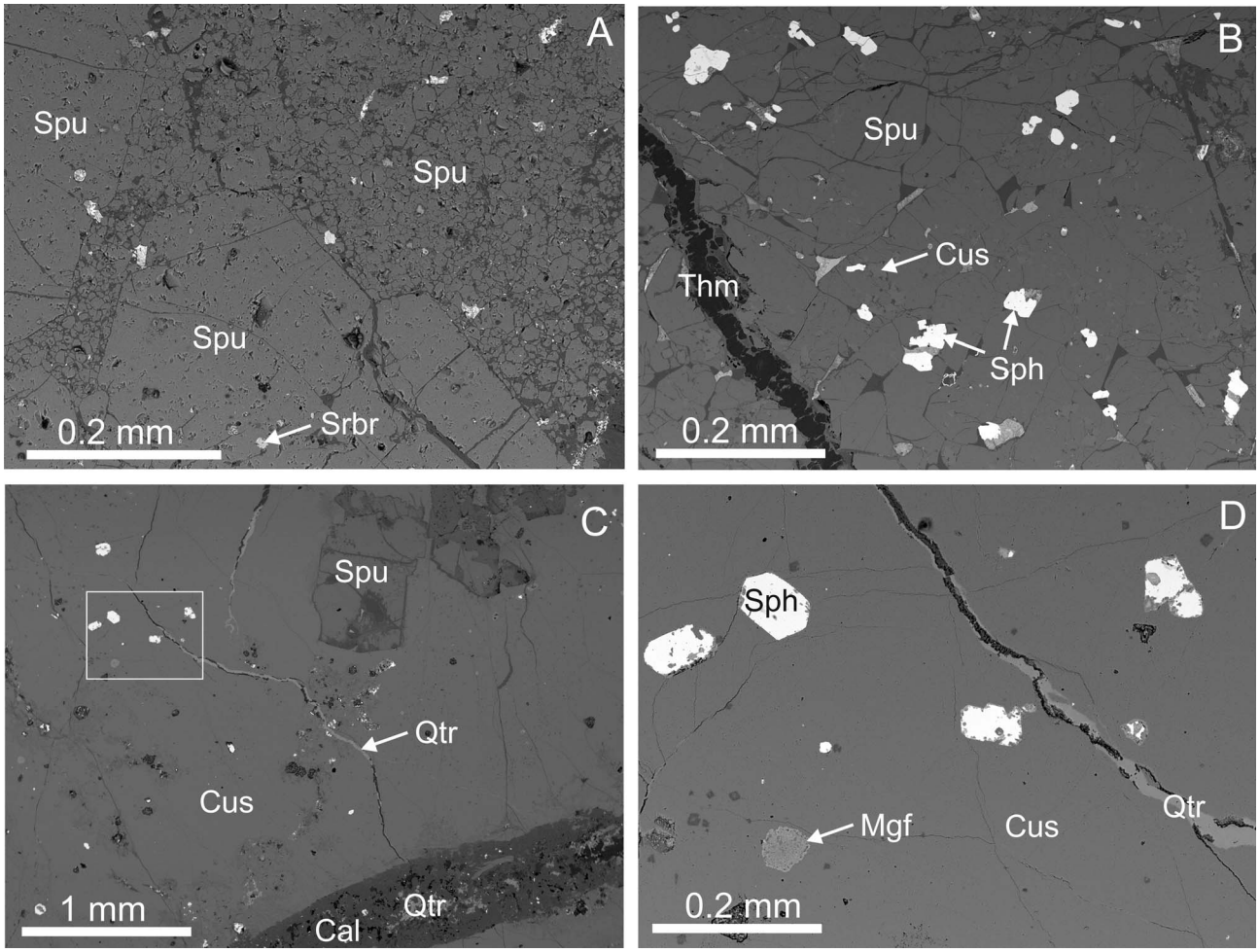

Fig. 2. (A) Poikilitic crystals of spurrite in a groundmass of fine-grained spurrite rock. Bright grains are sphalerite intergrown with altered Ca–Fe-sulfides and Cu–Fe–Ni-selenides. (B) Recrystallized fragments of spurrite rock. Light-grey grains consist of altered Ca–Fe-sulfides and Cu–Fe–Ni-selenides. (C) Relics of partially replaced metacrysts of spurrite in cuspidine zone with qatranaite-bearing veins. Fragment magnified in Fig. 2D is shown in the frame. (D) Metacrysts of magnesioferrite and sphalerite in cuspidine zone.

5. Composition and structure of qatranaite

Qatranaite crystals are chemically homogeneous and contain no other elements within the detection limits of microprobe analyses (Table 1), which leads to the end-member formula $CaZn_2(OH)_6{\cdot}2H_2O$. The presence of H_2O and (OH) groups is strongly supported by both Raman spectroscopy and structure determination.

Structural data were obtained for a crystal 0.09 × 0.04 × 0.03 mm^3 at 293(2) K. Experimental data and the results of structure refinement are given in Tables 2–5. The crystal structure of qatranaite corresponds to that of its synthetic equivalent (Fig. 5; Stahl & Jacobs, 1997; Xavier *et al.*, 2009). The $CaZn_2(OH)_6{\cdot}2H_2O$ compound contains Zn^{2+} tetrahedrally coordinated by OH^-, and Ca^{2+} octahedrally coordinated by four OH^- and two H_2O (Fig. 5). The Zn-centred tetrahedra form corner-sharing pyroxene-like chains, $Zn_2(OH)_6^{2-}$, between which the $Ca(OH_2)_2^{2+}$ groups are located (Fig. 5). The Ca and Zn polyhedra share the protonated oxygens O2 and O3; the protonated O1 is a bridging oxygen in the pyroxene-like chain (Fig. 5). The O4 oxygen bonds with Ca and H4 and H5, being so involved in the formation of the H_2O group (Fig. 5B). A system of hydrogen bonds significantly contributes to the stability of the qatranaite structure (Fig. 5). The geometry of the hydrogen bonds and bond valence sum (BVS) calculations are shown in Tables 6 and 7, respectively. The strong hydrogen bonds with $d_{O–O}$ (donor–acceptor distance) of 2.7 Å are characteristic for water molecules having a specific angle equal to 104 (2)° ($O_1\cdots H_4–O_4–H_5\cdots O_3$ configuration, Table 6). These hydrogen bonds have significant contributions to BVS for O1 and O3 oxygens (Table 7). Less strong hydrogen bonds with $d_{O–O}$ = 2.8–2.9 Å are related to $O_1–H_1\cdots O_2$ and $O_3–H_3\cdots O_4$ configurations (Table 6, Fig. 5) and have relatively less contributions to BVS for O2 and O4 (Table 7). The H2 atom forming an OH group with O2 oxygen is connected by very weak hydrogen bonds with neighbouring oxygens ($d_{O–O}$ > 3.3 Å, Table 6; hydrogen bonds are not shown in Fig. 5) and these bonds have vanishingly small contributions to BVS of neighbouring oxygens (Table 7).

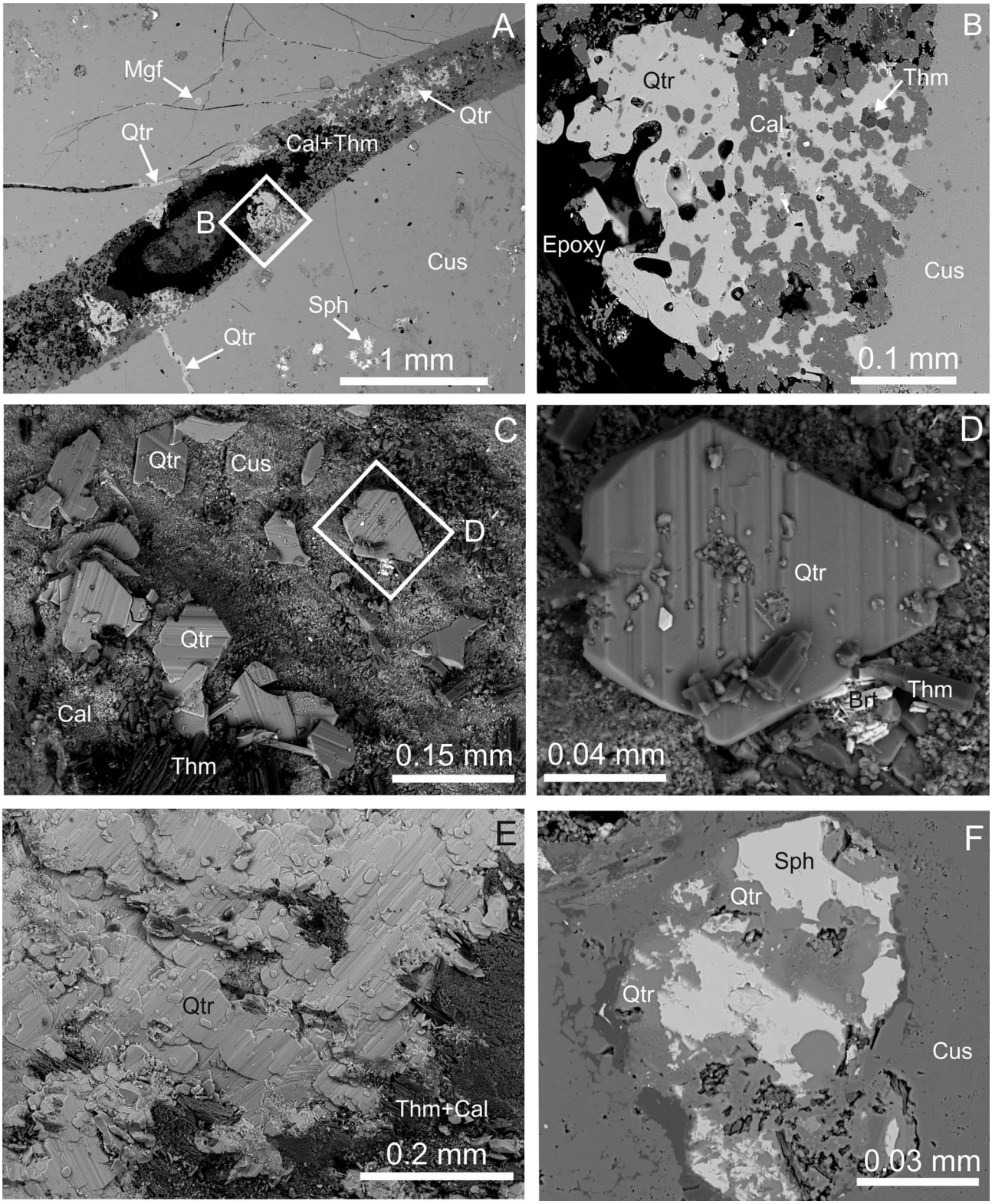

Fig. 3. (A) Low-temperature calcite–qatranaite–thaumasite veins in fine-grained cuspidine zone with abundant small sphalerite grains. Fragment magnified in Fig. 3B is shown in frame. (B) Qatranaite poikilocrystal with calcite, afwillite and thaumasite inclusions. (C) Qatranaite crystals and thaumasite on fracture surface in cuspidine zone; crystal magnified in Fig. 3D is shown in frame. (D) Qatranaite crystal with characteristic striation. (E) Parallel intergrowths of qatranaite crystals. (F) Sphalerite partially replaced by qatranaite. Qtr = qatranaite; Cal = calcite; Thm = Se-bearing thaumasite; Cus = cuspidine; Sph = sphalerite.

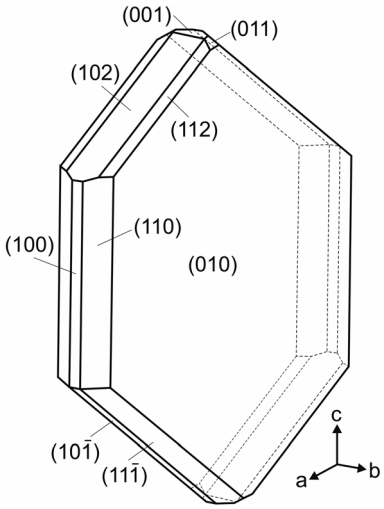

Fig. 4. Ideal crystal of qatranaite.

6. Raman spectroscopy

The Raman spectrum of qatranaite is characterised by the presence of the following bands (in cm^{-1}, Fig. 6, main lines are shown by bold): 215, **252**, 280, **297**, **344**, 385, **440**, 449, **479**, 526, 655, 780, 830, 877, **990**, **1065**, 1612, 2910, 3025, **3190**, 3210, **3497**, **3624**. The main bands in the Raman spectrum of qatranaite are related to the vibrations in $Zn(OH)_4^{2-}$ tetrahedra (cm^{-1}): 252, 297, 344 ($\nu_2 + \nu_4$, the possible contribution of Ca–O vibrations within Ca $(OH)_4(OH_2)_2^{2-}$ octahedra); 440, 449, 479 ($\nu_1 + \nu_3$); 990 (νZn–O–Zn); 1065 (νZn–O–H) (Lin *et al.*, 1995; Kesić *et al.*, 2015).

Strong bands at 3497 and 3624 cm^{-1} are related to stretching O–H vibrations. A more detailed fitting analysis allows us to divide the band at 3497 cm^{-1} into two components located at the same wavenumber but with different full width at half maximum (FWHM; Fig. 6). These bands are ascribed to the O3–H3···O4 configuration with d_{O-O} = 2.91 Å and the O1–H1···O2 configuration with d_{O-O} = 2.80 Å (Table 6, Fig. 5). The band at 3624 cm^{-1} corresponds to O2–H2···O1/O2/O3 geometry with $d_{O-O} > 3.3$ Å (Table 6) defining the very weak hydrogen bonds. Bands between ~2700–3480 cm^{-1} with relatively large FWHM centred about 2910, 3025, 3190 cm^{-1} are related to stretching vibrations of O–H in H_2O (Fig. 5; Lin *et al.*, 1995; Kesić *et al.*, 2015). The position of bands between ~2700 and ~3480 cm^{-1} indicates the presence of strong hydrogen bonds corresponding to the O1···H4–O4−H5···O3 configuration, with the donor–acceptor distances: O4–O1 = 2.71 Å and O4–O3 = 2.70 Å (Fig. 5; Table 6). The very weak band at 1612 cm^{-1} originated from bending vibrations of H_2O (Fig. 6; Lin *et al.*, 1995).

7. Discussion

Qatranaite was found only in the one outcrop of spurrite marble in the northern part of the Siwaqa pyrometamorphic terrain in Jordan. It was detected in low-temperature veins associated with "cuspidinised" parts of the rocks (Figs. 2C, D and 3A).

Pyrometamorphic rocks of the Siwaqa area, represented mainly by apatite-bearing spurrite marbles, have anomalously high contents of Cd, Zn, Mo, Ni, V, Cr and U inherited from the sedimentary protolith (Fleurance *et al.*, 2013; Khoury *et al.*, 2014; Abzalov *et al.*, 2015; Sokol *et al.*, 2017). Zinc in pyrometamorphic rocks occurs principally in sulfides (sphalerite is predominant), less frequently in selenides and in oxides (zincite, tululite), and also as negligible impurity in periclase, spinel and minerals of the (Ca, Cd)O series (Khoury *et al.*, 2016a and b).

Pyrometamorphic rocks of Jordan were investigated as an analogue of a geological repository for radioactive wastes (Khoury *et al.*, 1992; Fourcade *et al.*, 2007; Milodowski *et al.*, 2011; Martin *et al.*, 2016). It was established that infiltrating groundwater interacting with "clinker" pyrometamorphic phases produced a portlandite-buffered hyper-alkaline leachate plume that emanates from the "cement zone", and leads to the formation of hydrated cement phases such as ettringite, thaumasite, tobermorite, afwillite and jennite (Martin *et al.*, 2016). Previous work has demonstrated that saturation of natural cement-like rocks with groundwater

Table 2. Data collection and structure-refinement details for qatranaite.

Crystal system	Monoclinic
Crystal data	
Unit-cell dimensions	a = 6.3889(8) Å b = 10.9692(14) Å c = 5.7588(8) Å β = 101.949(14)°
Space group	$P2_1/c$ (no. 14)
Volume (Å^3)	394.84(9) Å^3
Z	2
Density (calculated)	2.598 g/cm^3
Chemical formula	$CaZn_2(OH)_6{\cdot}2H_2O$
Crystal size (mm)	0.09 × 0.04 × 0.03
Data collection	
Diffractometer SuperNova	
X-ray radiation	Mo$K\alpha$/0.71073 Å
X-ray power	50 kV, 0.8 mA
Monochromator	mirror monochromator
Temperature	293(2) K
Max. θ°-range	39.81°
Index ranges	$-11 \le h \le 11$ $-19 \le k \le 9$ $-10 \le l \le 10$
Measured reflections	14191
Unique reflections	2277
Observed reflections ($I > 2\sigma$ (I))	1528
Refinement of the structure	
No. of parameters	58
*R*int	0.0794
*R*σ	0.0581
*R*1. $I > 2\sigma(I)$	0.0377
*R*1 all data	0.0768
w*R*2 on (F^2)	0.0623
GooF	0.976
Δρ min, max (−e.Å^{-3})	−0.80, 0.74

Table 3. Atomic coordinates and displacement parameters (U_{eq}, in Å^2) for qatranaite.

Site	Atom	*x*	*y*	*z*	U_{eq}	sof
Zn	Zn	0.53316(4)	0.16497(2)	0.16389(4)	0.01485(7)	1
Ca	Ca	0	0	0	0.01362(11)	1
O1	O	0.4686(2)	0.18122(14)	0.8120(3)	0.0168(3)	1
O2	O	0.3378(3)	0.04282(14)	0.2461(3)	0.0175(3)	1
O3	O	0.8352(2)	0.12343(15)	0.2399(3)	0.0185(3)	1
O4	O	0.0375(3)	0.16029(14)	0.7367(3)	0.0206(3)	1
H1	H	0.539(4)	0.1190(16)	0.762(5)	0.025	1
H2	H	0.331(5)	0.061(3)	0.3966(17)	0.026	1
H3	H	0.876(5)	0.107(3)	0.3960(11)	0.028	1
H4	H	0.1773(12)	0.179(3)	0.759(6)	0.031	1
H5	H	0.971(4)	0.2329(12)	0.732(6)	0.031	1

Table 4. Anisotropic displacement parameters (Å^2) for qatranaite.

	U^{11}	U^{22}	U^{33}	U^{23}	U^{13}	U^{12}
Zn	0.01235(10)	0.01463(12)	0.01731(11)	−0.00066(10)	0.00252(8)	−0.00034(9)
Ca	0.0114(2)	0.0134(2)	0.0157(2)	−0.0004(2)	0.00180(19)	0.00002(19)
O1	0.0171(7)	0.0155(7)	0.0180(7)	0.0021(6)	0.0039(6)	0.0006(6)
O2	0.0164(7)	0.0191(7)	0.0167(7)	−0.0011(6)	0.0027(5)	−0.0029(6)
O3	0.0131(7)	0.0224(8)	0.0194(7)	−0.0030(6)	0.0020(6)	0.0018(6)
O4	0.0186(7)	0.0176(8)	0.0247(8)	0.0031(6)	0.0023(6)	0.0000(6)

Table 5. Selected interatomic distances (Å) for qatranaite.

Atom–	atom	Distance	Atom–	atom	Distance
Zn	O3	1.942(2)	O1	H1	0.899(2)
	O2	1.955(2)	O2	H2	0.899(2)
	O1	1.972(2)	O3	H3	0.900(2)
	O1	1.990(2)	O4	H4	0.900(2)
Ca	O3	2.335(2) × 2	O4	H5	0.899(2)
	O4	2.366(2) × 2			
	O2	2.371(2) × 2			

produces a hyper-alkaline pore fluid with a pH in the range 10–13.5 (Khoury *et al*., 1992; Techer *et al*., 2006).

Crystallization of qatranaite in cuspidine zones (Figs. 2C, D and 3A, B) and clinohedrite in hydrated fragments of spurrite marbles (Fig. S1A in Supplementary Material) took place after thaumasite and calcite vein formation and was accompanied by replacement of neighbouring sphalerite grains (Fig. 3F; S1B). Thaumasite stability (Jallad *et al*., 2003; Matschei & Glasser, 2015) indicates that qatranaite and clinohedrite in natural systems formed from highly alkaline solutions at temperature lower than 70 °C. Formation of artificial "qatranaite" in experiment on zinc sorption on cement materials took place at pH higher than 12 (Ziegler *et al*., 2001).

Clinohedrite, $CaZn(SiO_4){\cdot}H_2O$, formation is accompanied by spurrite dissolution (Fig. S1), which raises Ca and Si concentrations in the solution and promotes the crystallization of a Zn silicate with a Ca:Zn ratio of 1:1. In qatranaite, $CaZn_2(OH)_6{\cdot}2H_2O$, Ca:Zn = 1:2; its crystallization in veins follows the formation of thaumasite and calcite, which caused Ca and Si contents decrease in the solution.

"Cuspidinisation" of spurrite rocks is a necessary condition for qatranaite veins formation and for this reason requires a discussion. Cuspidine is a relatively high-temperature mineral, stable in hydrothermal systems up to 800 °C (Van Valkenburg & Rynders, 1958) and in melt systems up to 1400–1600 °C (Watanabe *et al*., 2002). The presence of magnesioferrite metacrysts in cuspidine zones (Fig. 2D) indicates that their temperature of formation was not lower than 800 °C (Guo & Guo, 2017). Consequently, cuspidine veins formation occurred in the temperature range 800–850 °C, at which the spurrite marble of Hatrurim Complex formed (Khoury *et al*., 2016a and b). The mechanism of cuspidine-zone formation can be described as follows: At the first stage of combustion metamorphism, typical spurrite marble was formed and, as a consequence of rock cooling and partial leaching, thermal fissures appeared. These fissures/cracks were a pathways system, in which circulating heated fluids (gas) were keeping temperature high along the fractures. In non-fractured areas, typical fine-grained spurrite marble remained unaffected. At the periphery of the blocks, conditions required for spurrite recrystallization were kept during extended time, allowing the growth of relatively large spurrite metacrysts (Fig. 2A). Fluids (gases) are by-products of combustion processes and they are likely generated in nearby combustion foci. Similar formation of large spurrite metacrysts was noted in altered spurrite rocks of the Hatrurim Complex in the Negev Desert, Israel, which are characterized by high rock-fracturation, presence of

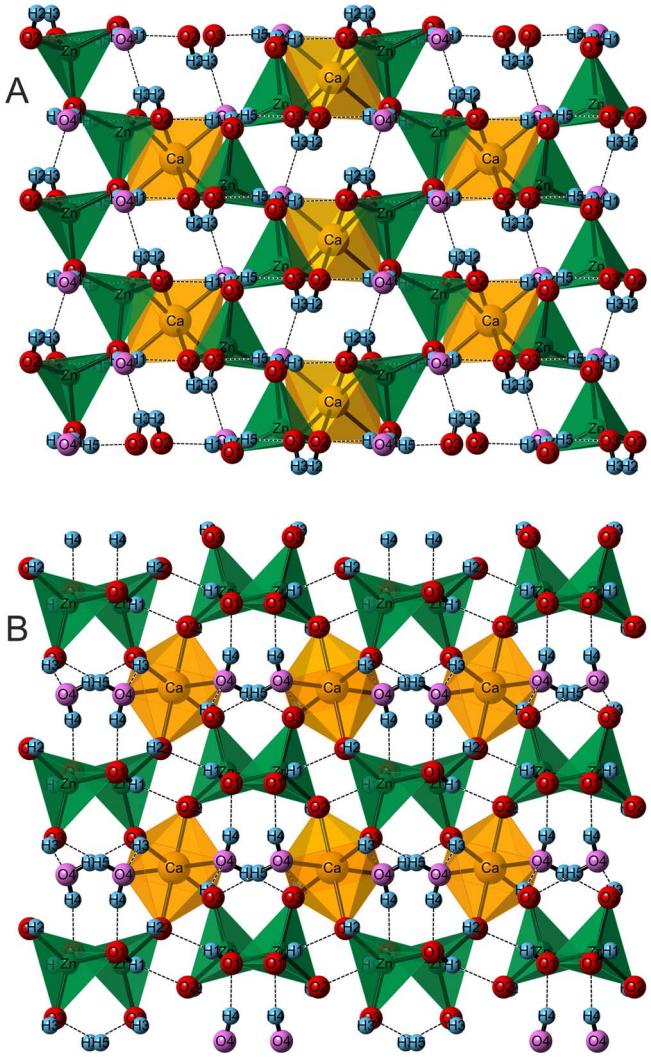

Fig. 5. The crystal structure of qatranaite. (A) (100) projection, (B) (001) projection. The Ca atoms form $Ca(OH_2)_2^{2+}$ groups (or $[Ca(OH)_4(OH_2)_2]$ octahedra), between $[Zn_2(OH)_6]^{2-}$ pyroxene-like chains. Zn-tetrahedra – green, Ca-octahedra – orange, oxygen – red balls, hydrogen – blue balls; oxygens belonging to the H_2O groups – pink balls. The strong hydrogen bonds are marked with dashed lines.

gaseous channels (fumaroles) as well as occurrence of stracherite, $BaCa_6(SiO_4)_2[(PO_4)(CO_3)]F$, and ariegilatite, $BaCa_{12}(SiO_4)_4(PO_4)_2F_2O$, metacrysts (Galuskin *et al.*, 2018a and b). When the chemical character of fluids changed (from carbonate-bearing to fluorine-bearing), spurrite at high-temperature conditions was replaced by cuspidine at the periphery of the blocks. Subsequently, the cuspidine zones became the substrate for low-temperature mineral formation involving qatranaite.

Table 7. Bond-valence calculations for qatranaite (valence units).

	O1	O2	O3	O4	Sum
Ca		0.34 × 2→	0.37 × 2→	0.34 × 2→	2.10
Zn	0.46	0.51	0.53		1.98
	0.48				
H1	0.74	0.23			0.97
H2	0.03	0.74			0.77
		0.02			
H3			0.74	0.15	0.89
H4	0.33			0.74	1.07
H5			0.34	0.74	1.08
Sum	2.04	1.84	1.95	1.97	

Bond-valence parameters for H–O taken from Yua *et al.* (2006), Zn–O and Ca–O taken from Brown & Altermatt (1985).

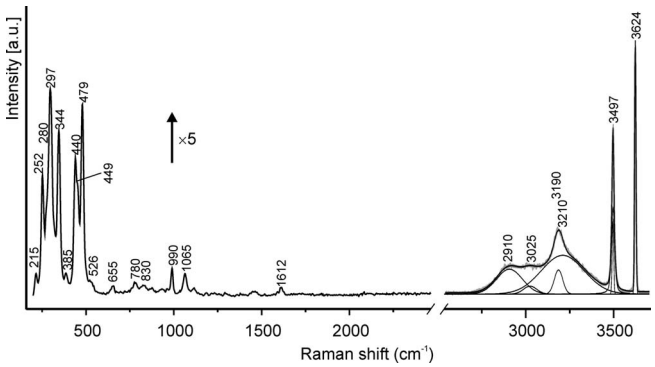

Fig. 6. Raman spectrum of qatranaite.

Acknowledgements: The authors thank E. Sokol and anonymous reviewers for their careful revision that improved the early version of the manuscript. The investigations were partially supported by the National Science Centre (NCN) of Poland, grant no. 2016/23/B/ST10/00869.

Table 6. Geometry of hydrogen bonds and calculated Raman modes of qatranaite.

Configuration	$d(O_d–O_a)$/Å	$d(O_d–H)$/Å	$d(H\cdots O_a)$/Å	O–H···O angle (°)	Calculated Raman modes (cm^{-1})
$O_1\cdots H_4–O_4–H_5\cdots O_3$[a]	$O_4–O_3$ = 2.70(1)	$O_4–H_4$ = 0.90(1)	$H_4\cdots O_1$ = 1.82(1)	177(2)	~3190[b]
	$O_4–O_1$ = 2.71(1)	$O_4–H_5$ = 0.90(1)	$H_5\cdots O_3$ = 1.80(1)	168(2)	~3220[b]
$O_1–H_1\cdots O_2$	$O_1–O_2$ = 2.80(1)	$O_1–H_1$ = 0.90(1)	$H_1\cdots O_2$ = 1.95(1)	159(2)	~3400[b]
$O_3–H_3\cdots O_4$	$O_3–O_4$ = 2.91(1)	$O_3–H_3$ = 0.90(1)	$H_3\cdots O_4$ = 2.10(1)	149(2)	~3510[b]
$O_2–H_2\cdots O_1/O_2/O_3$	$O_2–O$ > 3.3	$O_2–H_2$ = 0.90(1)	$H_2\cdots O$ > 2.7	~90–150	>3600

[a]H–O–H angle = 104(2)°;
[b]$\nu(cm^{-1}) = 3592 – 304 \times 10^9 \times \exp(-d(O–O)/0.1321)$ (Libowitzky, 1999).

References

Abzalov, M.Z., Heyden, A. van der, Saymeh, A., Abuqudaira, M. (2015): Geology and metallogeny of Jordanian uranium deposits. *Appl. Earth Sci.*, **124**, 63–77.

Alqudah, M., Ali Hussein, M., van den Boorn, S., Podlaha, O.G., Mutterlose, J. (2015): Biostratigraphy and depositional setting of Maastrichtian–Eocene oil shales from Jordan. *Mar. Petrol. Geol.*, **60**, 87–104.

Alsharhan, A.S. & Nairn, A.E.M. (2003): Sedimentary basins and petroleum geology of the Middle East. Elsevier, Amsterdam, 943 p.

Barijous, M.O. (1985): Geological Map of Jordan (1: 50,000, Siwaqa). Sheet 3252-IV.

Bentor, Y. (1960): Israel. *in* "Lexique Stratigraphique International, vol. III, part 10.2, Asie", Centre National de la Recherche Scientifique, Paris, 80 p.

Britvin, S.N., Murashko, M.N., Vapnik, Y., Polekhovsky, Y.S., Krivovichev, S.V. (2015): Earth's phosphides in Levant and insights into the source of Archean prebiotic phosphorus. *Sci. Rep.*, **5**, 08355. https://doi.org/10.1038/srep08355.

Britvin, S.N., Murashko, M.N., Vapnik, Y., Polekhovsky, Y.S., Krivovichev, S.V., Vereshchagin, O.S., Vlasenko, N.S., Shilovskikh, V.V., Zaitsev, A.N. (2018): Zuktamrurite, FeP_2, a new mineral, the phosphide analogue of löllingite, $FeAs_2$. *Phys. Chem. Minerals*. https://doi.org/10.1007/s00269-018-1008-4.

Brown, I.D. & Altermatt, D. (1985): Bond-valence parameters obtained from a systematic analysis of the inorganic crystal structure database. *Acta Crystallogr.*, **B41**, 244–247.

Caldeira, V., Jouffret, L., Thiel, J., Lacoste, F.R., Obbade, S., Dubau, L., Chatenet, M. (2017): Ultrafast hydro-micromechanical synthesis of calcium zincate: Structural and morphological characterizations. *J. Nanomater.*, 1–8. ID 7369397.

Fleurance, S., Cuney, M., Malartre, F., Reyx, J. (2013): Origin of the extreme polymetallic enrichment (Cd, Cr, Mo, Ni, U, V, Zn) of the Late Cretaceous–Early Tertiary Belqa Group, central Jordan. *Palaeogeogr. Palaeoclimatol. Palaeoecol.*, **369**, 201–219.

Fourcade, S., Trotignon, L., Boulvais, P., Techer, I., Vandamme, E.M., Salameh, D., Khoury, H. (2007): Cementation of kerogen-rich marls by alkaline fluids released during weathering of thermally metamorphosed marly sediments. Part I: Isotopic (C, O) study of the Khushay Matruk natural analogue (central Jordan). *Appl. Geochem.*, **22**, 1293–1310.

Galuskin, E.V., Gfeller, F., Armbruster, T., Galuskina, I.O., Vapnik, Ye., Murashko, M., Włodyka, R., Dzierżanowski, P. (2015): New minerals with modular structure derived from hatrurite from the pyrometamorphic Hatrurim Complex, Part I: Nabimusaite, $KCa_{12}(SiO_4)_4(SO_4)_2O_2F$, from larnite rock of the Jabel Harmun, Palestinian Autonomy, Israel. *Mineral. Mag.*, **79**, 1061–1072.

Galuskin, E.V., Galuskina, I.O., Gfeller, F., Krüger, B., Kusz, J., Vapnik, Y., Dulski, M., Dzierżanowski, P. (2016): Silicocarnotite, $Ca_5[(SiO_4)(PO_4)](PO_4)]$, a new, old'' mineral from the Negev Desert, Israel, and the ternesite–silicocarnotite solid solution: Indicators of high-temperature alteration of pyrometamorphic rocks of the Hatrurim Complex, Southern Levant. *Eur. J. Mineral.*, **28**, 105–123.

Galuskin, E.V., Krüger, B., Galuskina, I.O., Krüger, H., Vapnik, Ye., Pauluhn, A., Olieric, V. (2018a): Stracherite, $BaCa_6(SiO_4)_2[(PO_4)(CO_3)]F$, a first CO_3-bearing intercalated hexagonal antiperovskite from Negev Desert, Israel. *Am. Mineral.*, **103**, 1699–1706.

Galuskin, E.V., Krüger, B., Galuskina, I.O., Krüger, H., Vapnik, Y., Wojdyla, J.A., Murashko, M. (2018b): New mineral with modular structure derived from hatrurite from the pyrometamorphic rocks of the Hatrurim Complex: Ariegilatite, $BaCa_{12}(SiO_4)_4(PO_4)_2F_2O$, from Negev Desert, Israel. *Minerals*, **8**, 109.

Galuskina, I.O., Galuskin, E.V., Armbruster, T., Lazic, B., Kusz, J., Dzierżanowski, P., Gazeev, V.M., Pertsev, N.N., Prusik, K., Zadov, A.E., Winiarski, A., Wrzalik, R., Gurbanov, A.E. (2010): Elbrusite-(Zr) – a new uranian garnet from the Upper Chegem caldera, Kabardino-Balkaria, Northern Caucasus, Russia. *Am. Mineral.*, **95**, 1172–1181.

Galuskina, I.O., Vapnik, Y., Lazic, B., Armbruster, T., Murashko, M., Galuskin, E.V. (2014): Harmunite $CaFe_2O_4$: A new mineral from the Jabel Harmun, West Bank, Palestinian Autonomy, Israel. *Am. Mineral.*, **99**, 965–975.

Geller, Y.I., Burg, A., Halicz, L., Kolodny, Y. (2012): System closure during the combustion metamorphic "Mottled Zone" event, Israel. *Chem. Geol.*, **334**, 25–36.

Gross, S. (1977): The mineralogy of the Hatrurim Formation, Israel. *Geol. Surv. Israel Bull.*, **70**, 1–80.

Guo, Y.-F. & Guo, X.-M. (2017): Formation of $[Mg_{1-x}, Fe_x]O$ Fe_2O_3 in solid-state reactions between MgO and Fe_2O_3 in the Fe_2O_3-rich system. *ISIJ Intern.*, **57**, 228–235.

Jallad, K.N., Santhanam, M., Cohen, M.D. (2003): Stability and reactivity of thaumasite at different pH levels. *Cem. Conc. Res.*, **33**, 433–437.

Kesić, Ž., Lukić, I., Zdujić, M., Jovalekić, Č., Liu, H., Skala, D. (2015): Mechanochemical synthesis of $CaO{\cdot}ZnO{\cdot}K_2CO_3$ catalyst: Characterization and activity for methanolysis of sunflower oil. *Chem. Ind. Chem. Eng.*, **21**, 1–12.

Khoury, H.N., Salameh, E., Clark, I.D., Fritz, P., Baljjali, W., Milodowski, A. E., Cave, M.R., Alexander, W.R. (1992): Natural analogue of high pH cement pore waters from the Maqarin area of northern Jordan. I: Introduction to the site. *J. Geoch. Expl.*, **46**, 117–132.

Khoury, H.N., Salameh, E.M., Clark, I.D. (2014): Mineralogy and origin of surficial uranium deposits hosted in travertine and calcrete from central Jordan. *Appl. Geochem.*, **43**, 49–65.

Khoury, H.N., Sokol, E.V., Kokh, S.N., Seryotkin, Y.V., Kozmenko, O.A., Goryainov, S.V., Clark, I.D. (2016): Intermediate members of the lime-monteponite solid solutions ($Ca_{1-x}Cd_xO$, x = 0.36–0.55): Discovery in natural occurrence. *Am. Mineral.*, **101**, 146–160.

Khoury, H.N., Sokol, E.V., Nigmatulina, E.N., Goryainov, S.V., Belogub, E.V., Clark, I.D. (2016): Tululite, $Ca_{14}(Fe^{3+}, Al)(Al, Zn, Fe^{3+}, Si, P, Mn, Mg)_{15}O_{36}$: A new Ca zincate-aluminate from combustion metamorphic marbles, central Jordan. *Mineral. Petrol.*, **110**, 125–140.

Kolodny, Y., Burg, A., Sneh, A. (2013): Comment on "Combustion metamorphism (CM) in the Nabi Musa dome: New implications for a mud volcanic origin of the Mottled Zone, Dead Sea area", by: E. Sokol, I. Novikov, S. Zateeva, Ye. Vapnik, R. Shagam and O. Kozmenko, Basin Research (2010) 22, 414–438. *Basin Res.*, **25**, 112–114.

Kolodny, Y. & Gross, S. (1974): Thermal metamorphism by combustion of organic matter: Isotopic and petrological evidence. *J. Geol.*, **82**, 489–506.

Libowitzky, E. (1999): Correlation of O-H stretching frequencies and O-H...O hydrogen bond lengths in minerals. *Monatsh. Chem.*, **130**, 1047–1059.

Lin, T.-C., Mollah, M.Y.A., Vempati, R.K., Cocke, D.L. (1995): Synthesis and characterization of calcium hydroxyzincate using X-ray diffraction, FT-IR spectroscopy, and scanning force microscopy. *Chem. Mater.*, **7**, 1974–1978.

Martin, L.H.J., Leemann, A., Milodowski, A.E., Mäder, U.K., Münch, B., Giroud, N. (2016): A natural cement analogue study to understand the long-term behaviour of cements in nuclear waste repositories: Maqarin (Jordan). *Appl. Geochem.*, **71**, 20–34.

Matschei, T. & Glasser, F.P. (2015): Thermal stability of thaumasite. *Mat. Struc.*, **48**, 2277–2289.

Matthews, A. & Gross, S. (1980): Petrologic evolution of the Mottled Zone (Hatrurim) metamorphic complex of Israel. *Israel J. Earth Sci.*, **29**, 93–106.

Milodowski, A.E., Trotignon, L., Khoury, H., Salameh, E., Arnal, N., Bienvenu, P., Bulle, C., Chenery, S.R., Crouzet, N., Fontanini, L., Hodgkinson, E.S., Mäder, U., McKervey, J., Peycelon, H., Pontremol, S., Rassineux, F., Raynal, J., Rose, J., Vandamme, D., Provitina, O., Raimbault, L., Pitty, A., Alexander, R. (2011): The analog cement zone (ACZ). *in* "A natural analog study of cement buffered, hyperalkaline groundwaters and their interaction with a Repository Host Rock IV: An examination of the Khushaym Matruk (central Jordan) and Maqarin (northern Jordan) sites, Chapter 4", NDA-RWMD Technical Report, NDA, Moors Row, U.K.

Novikov, I., Vapnik, E., Safonova, I. (2013): Mud volcano origin of the Mottled Zone, South Levant. *Geosci. Front.*, **4**, 597–619.

Powell, J. H. & Moh'd, B. K. (2011): Evolution of Cretaceous to Eocene alluvial and carbonate platform sequences in central and south Jordan. *GeoArabia*, **16** (4), 29–82.

Ropp, R.C. (2013): (Zn, Cd and Hg) alkaline earth compounds. *in* "Encyclopedia of the alkaline earth compounds", Elsevier, Amsterdam, 1115–1174.

Sheldrick, G.M. (2008): A short history of SHELX. *Acta Crystallogr.*, **A64**, 112–122.

Sokol, E., Novikov, I., Zateeva, S., Vapnik, Y., Shagam, R., Kozmenko, O. (2010): Combustion metamorphism in the Nabi Musa dome: New implications for a mud volcanic origin of the Mottled Zone, Dead Sea area. *Basin Res.*, **22**, 414–438.

Sokol, E.V., Kozmenko, O.A., Khoury, H.N., Kokh, S.N., Novikova, S.A., Nefedov, A.A., Sokol, I.A., Zaikin, P. (2017): Calcareous sediments of the Muwaqqar Chalk Marl Formation, Jordan: Mineralogical and geochemical evidences for Zn and Cd enrichment. *Gondwana Res.*, **46**, 204–226.

Stahl, R. & Jacobs, H. (1997): Zur Kristallstruktur von $CaZn_2(OH)_6$ $2H_2O$. *Z. Für Anorg. Allg. Chem.*, **623**, 1287–1289.

Techer, I., Khoury, H.N., Salameh, E., Rassineux, F., Claude, C., Clauer, N., Pagel, M., Lancelot, J., Hamelin, B., Jacquot, E. (2006): Propagation of high-alkaline fluids in an argillaceous formation: Case study of the Khushaym Matruk natural analogue (Central Jordan). *J. Geochem. Explor.*, **90**, 53–67.

Van Valkenburg, A. and Rynders, G.F. (1958): Synthetic cuspidine. *Am. Mineral.*, **43**, 1195–1202.

Vapnik, Y. & Novikov, I. (2013): Reply to Comment of Y. Kolodny, A. Burg and A. Sneh on "Combustion metamorphism in the Nabi Musa dome: New implications for a mud volcano origin of the Mottled Zone, Dead Sea area", by E. Sokol, I. Novikov, S. Zateeva, Ye. Vapnik, R. Shagam and O. Kozmenko, Basin Research (2010), 22, 414–438. *Basin Res.*, **25**, 115–120.

Vapnik, Y., Sharygin, V., Sokol, E., Shagam, R. (2007): Paralavas in a combustion metamorphic complex: Hatrurim Basin, Israel. *Geol. Soc. Am. Rev. Eng. Geol.*, **18**, 133–154.

Watanabe, T., Fukuyama, H., Nagata, K. (2002): Stability of cuspidine ($3CaO$ $2SiO_2$ CaF_2) and phase relations in the CaO–SiO2–CaF2 system. *ISIJ Intern.*, **42**, 489–497.

Xavier, C.S., Sczancoski, J.C., Cavalcante, L.S., Paiva-Santos, C.O., Varela, J.A., Longo, E., Li, M.S. (2009): A new processing method of $CaZn_2(OH)_6$ $2H_2O$ powders: Photoluminescence and growth mechanism. *Solid State Sci.*, **11**, 2173–2179.

Yang, C.-C., Chien, W.-C., Chen, P.-W., Wu, C.-Y. (2009): Synthesis and characterization of nano-sized calcium zincate powder and its application to Ni–Zn batteries. *J. Appl. Electrochem.*, **39**, 39–44.

Yua, D., Xuea, D., Ratajczak, H. (2006): Golden ratio and bond-valence parameters of hydrogen bonds of hydrated borates. *J. Mol. Struc.*, **783**, 210–214.

Zaitsev, A.N., Williams, C.T., Britvin, S.N., Kuznetsova, I.V., Spratt, J., Petrov, S.V., Keller, J. (2011): Kerimasite, $Ca_3Zr_2(Fe_2^{3+}$ $Si)O_{12}$, a new garnet from carbonatites of Kerimasi volcano and surrounding explosion craters, Northern Tanzania. *Mineral. Mag.*, **74**, 803–820.

Ziegler, M.A. (2001): Late Permian to Holocene paleofacies evolution of the Arabian plate and its hydrocarbon occurrences. *GeoArabia*, **6**, 445–504.

Ziegler, F., Gieré, R., Johnson, C. (2001): Sorption mechanisms of zinc to calcium silicate hydrate: Sorption and microscopic investigations. *Environ. Sci. Technol.*, **35**, 4556–4561.

Received 1 October 2018
Modified version received 25 December 2018
Accepted 1 January 2019